Revisiting the Canterbury earthquake sequence after the 14 February 2016 M_w 5.7 event

Matthew W. Herman[1] and Kevin P. Furlong[1]

[1]Department of Geosciences, Pennsylvania State University, University Park, Pennsylvania, USA

Abstract On 14 February 2016, an M_w 5.7 (GNS Science moment magnitude) earthquake ruptured offshore east of Christchurch, New Zealand. This earthquake occurred in an area that had previously experienced significant seismicity from 2010 to 2012 during the Canterbury earthquake sequence, starting with the 2010 M_w 7.0 Darfield earthquake and including four M_w ~6.0 earthquakes near Christchurch. We determine source parameters for the February 2016 event and its aftershocks, relocate the recent events along with the Canterbury earthquakes, and compute Coulomb stress changes resolved onto the recent events and throughout the greater Christchurch region. Because the February 2016 earthquake occurred close to previous seismicity, the Coulomb stress changes resolved onto its nodal planes are uncertain. However, in the greater Christchurch region, there are areas that remain positively loaded, including beneath the city of Christchurch. The recent earthquake and regional stress changes suggest that faults in these regions may pose a continuing seismic hazard.

1. Introduction

On 14 February 2016, an M_w 5.7 (GNS Science moment magnitude; http://www.geonet.org.nz/quakes/region/newzealand/2016p118944) earthquake ruptured offshore east of Christchurch on the South Island of New Zealand. This event occurred in the vicinity of the earlier Canterbury earthquake sequence, which began with the 3 September 2010 M_w 7.0 Darfield earthquake and included M_w ~6.0 events on 21 February, 13 June, and 23 December 2011 (Figure 1) [*Quigley et al.*, 2016, and references therein]. Following the decay of the aftershocks associated with the 23 December 2011 earthquake, seismicity in the region returned to a level of relative quiescence (~1.8 events M_L (GNS Science local magnitude) 2.0+ per day from June 2012 to February 2016; this rate is still substantially higher than the ~0.2 events per day before the 2010 earthquake; Figures 1b and 1c and S1 in the supporting information). From June 2012 to December 2014, there were no earthquakes larger than M_L 4.7, and from January 2015 up to the February 2016 event, there were no earthquakes larger than M_L 4.0.

Although the 2016 earthquake did not cause significant damage or casualties, it generated significant shaking, with measured peak ground accelerations of up to 36% g (http://info.geonet.org.nz/display/appdata/Strong-Motion+Data). It also suggests that residual increased seismic rupture probability remains in the general region of the Canterbury earthquake sequence, even years after the initial main shock and more than 4 years since the occurrence of the last significant event.

Placing this recent earthquake into context requires us to look back on the Canterbury earthquake sequence, revisit interpretations of kinematics, and reevaluate the implications for future seismotectonic activity in the Christchurch vicinity described during or soon after the completion of the main sequence [e.g., *Fry and Gerstenberger*, 2011; *Sibson et al.*, 2011; *Beavan et al.*, 2012; *Ristau et al.*, 2013; *Herman et al.*, 2014; *Steacy et al.*, 2014]. In this study, we explore the location of this recent event to assess whether it occurred in a seismic gap along one of the previously active fault strands of the Canterbury sequence or, alternatively, if it occurred on a distinctly separate, previously inactive structure. Earthquakes occurring in seismic gaps on active structures are generally thought to be constrained in size and location by the dimensions of the gap and the remaining slip deficit [e.g., *McCann et al.*, 1979; *Fialko*, 2006]. In contrast, if significant subsequent earthquakes occur on structures other than those associated with previously active faults, i.e., on faults that have not yet hosted significant seismic activity, then the population of faults that could possibly host a later earthquake is increased. Thus, the residual hazard after an earthquake sequence like the Canterbury sequence could remain higher than previously anticipated and be partly controlled by regional stress conditions and the number and size of available faults.
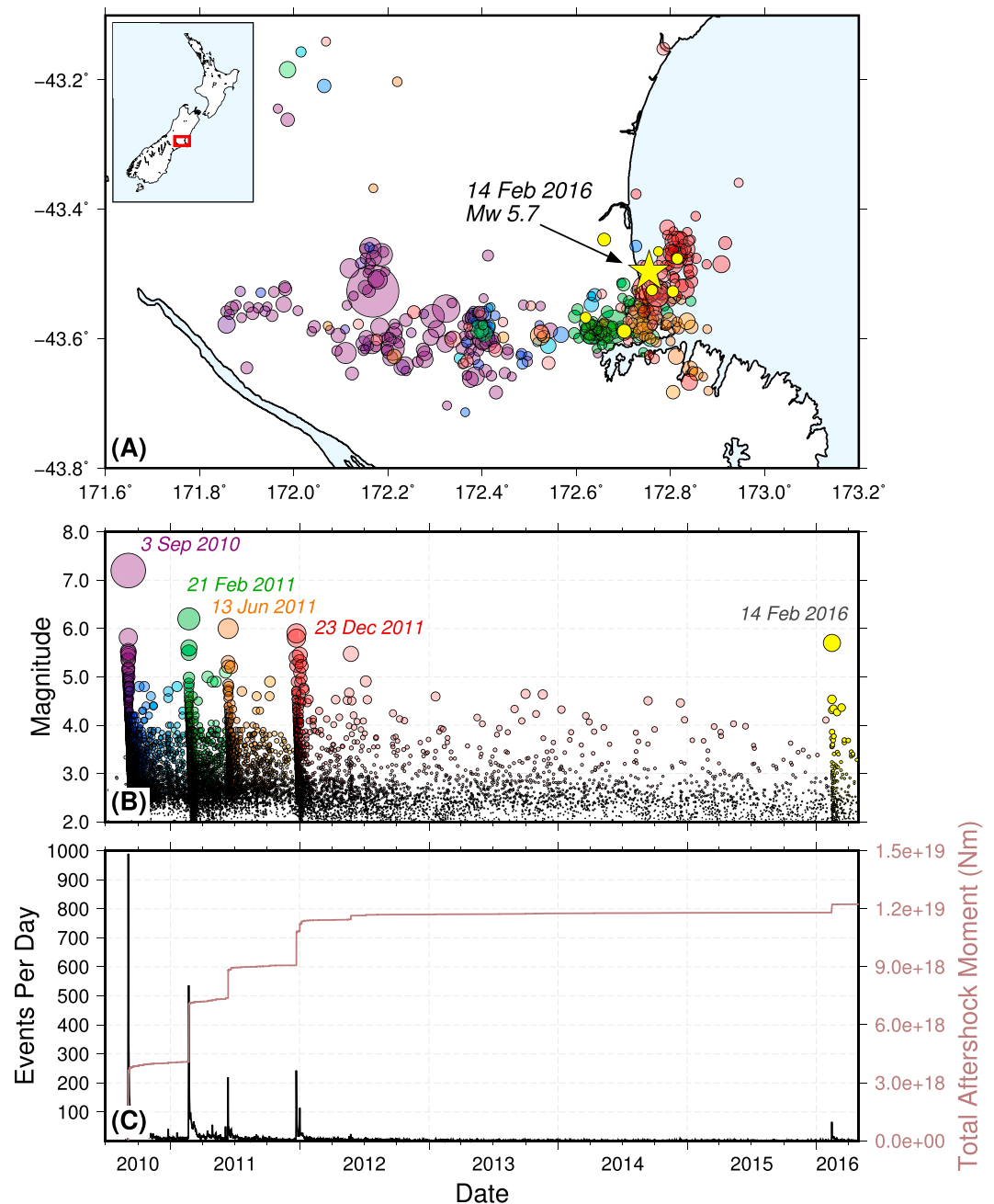
Figure 1. Seismicity in the Canterbury earthquake sequence from September 2010 to April 2016. (a) Earthquakes M_L 4.0 and larger, colored by rupture date and scaled by magnitude. The February 2016 event is indicated by a star. The mapped area is outlined in the inset. (b) Local magnitude versus time, starting with the M_w 7.0 (M_L 7.2) Darfield earthquake on 3 September 2010 through April 2016. Note the gap in significant earthquakes from 2013 to 2015. (c) Seismicity rate over time. The black curve shows the seismicity rate (number of events M_L 2.0 and larger per day), and the red curve shows the cumulative moment release of all recorded events following the M_w 7.0 Darfield main shock.

2. Methods

To analyze the February 2016 event and its aftershocks in comparison with earlier seismicity in the Canterbury Plains from 2010 to 2014, we determine earthquake fault parameters (strike, dip, rake, seismic moment/magnitude, and centroid depth) for 11 earthquakes from January 2014 to March 2016. For consistency with previous results, we implement the regional moment tensor (RMT) inversion technique described in *Herman et al.* [2014] and references therein. This algorithm uses the *Computer Programs in Seismology*
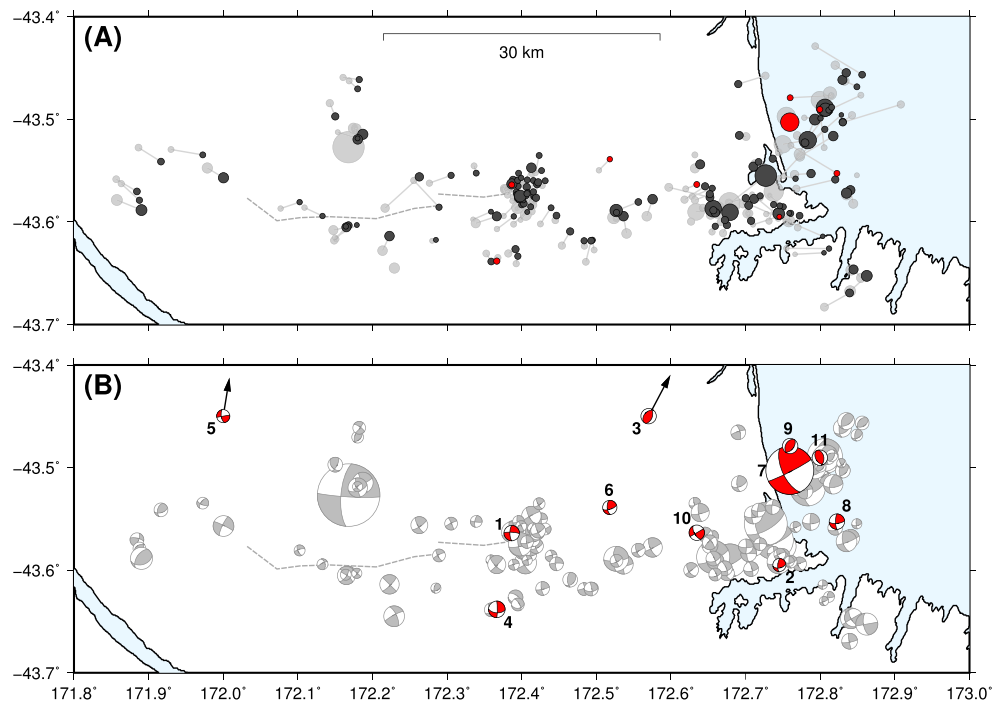
Figure 2. (a) Relative relocation results. The grey dots indicate the GNS Science locations of the 161 earthquakes for which we have computed regional moment tensor (RMT) solutions. The black dots are the relocated hypocenters of the 150 RMT solutions from *Herman et al.* [2014]. The red dots are the relocated hypocenters of the 11 RMT solutions determined in this study. (b) RMT solutions from *Herman et al.* [2014] in grey and solutions from this study in red. Solutions from this study have been slightly enlarged to emphasize the focal mechanisms. The label numbers correspond to the labels in the text and in Table 1. Events 3 and 5 occurred off the northern end of the mapped region.

software [*Herrmann*, 2013] to perform a grid search for the double-couple point source that best fits regional broadband waveforms from seismic stations on South Island, New Zealand [*Herrmann et al.*, 2011]. These waveforms are processed by (a) deconvolving to ground velocity in m/s; (b) rotating to vertical, radial, and transverse components; (c) truncating from 10 s before the *P* wave arrival to 120 s after the *P* wave arrival; and (d) band-pass filtering typically from 0.02 to 0.0625 Hz (50–16 s). The 14 February 2016 earthquake was large enough that it required a longer period passband (0.01–0.05 Hz) to maintain a point source approximation. Synthetic waveforms are generated using a regional South Island, New Zealand, velocity structure and are processed identically to the observed traces. This velocity model is the same as in our previous study and was derived from surface wave dispersion measurements at the same regional seismic stations [*Herman et al.*, 2014]. We are able to determine RMT solutions for earthquakes as small as M_w 3.6 and consistently determine solutions for nearly all events M_w 4.5 and larger. Fault planes are interpreted for all 161 RMT solutions based on the orientation of the nodal plane most closely aligned with nearby aftershock cluster orientations, although fault planes for some events remain ambiguous, particularly in the complex deformation regions near 172.4°E and 172.8°E (Figure 2) [*Herman et al.*, 2014].

The double-difference hypocenter relocation software *hypoDD* [*Waldhauser and Ellsworth*, 2000] is used to determine relative locations of all 161 earthquakes with RMT solutions, from the September 2010 Darfield earthquake to the most recent aftershock of the February 2016 event in March 2016. We picked 3833 *P* wave arrivals from the vertical components of local strong motion and regional broadband stations and 1784 *S* wave arrivals from the transverse components of regional broadband stations. *P* wave picks are assigned a weight of 1.0, while *S* wave picks are assigned a weight of 0.2, reflecting greater uncertainty in the shear wave arrival time. The locations used to initialize *hypoDD* are the GNS Science hypocenters. Multiple configurations of the *hypoDD* event-linking and inversion schemes were used to test the robustness of the relative relocation solutions.

Static stress changes are computed by placing the earthquakes in an elastic half-space and using a code written by the authors to apply the equations of *Okada* [1992]. We treat all of the sources as having finite fault areas. The 2010 Darfield main shock geometry and slip distribution is defined by published finite fault models
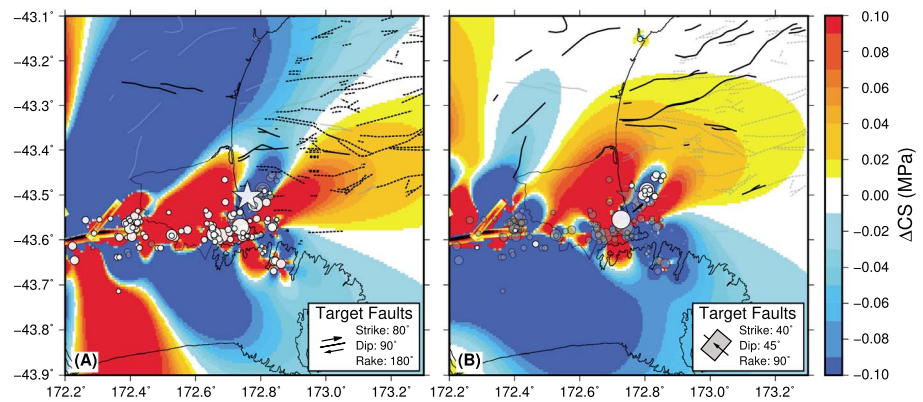
Figure 3. Coulomb stress change (ΔCS) in the Canterbury Plains generated by all 161 earthquakes in the RMT catalog from this study, resolved at 10 km depth. The 2010 Darfield main shock slip is the *Beavan et al.* [2012] solution, which is based on geodetic observations. Using a different slip model [e.g., *Hayes*, 2010] changes the details of the ΔCS distribution near the fault but not the general pattern (Figure S2). The white symbols are the earthquakes with the same kinematics as the target faults. Note that many of the white symbols occur in blue regions because they have reduced the nearby ΔCS as a result of their rupture. The transparent dark symbols are the earthquakes with different mechanisms in the sequence. The solid lines are the mapped faults interpreted to have the same kinematics as the target faults, and the dotted lines are interpreted as normal faults but may accommodate oblique or strike-slip deformation (fault data courtesy of NIWA [*Barnes et al.*, 2016]). The star indicates the location of the 14 February 2016 M_w 5.7 earthquake, and an outline of Christchurch city is shown for reference. (a) ΔCS resolved onto right-lateral strike-slip faults with a strike of 80°, like one of the nodal planes of the February 2016 event. This pattern is nearly the same as the ΔCS resolved onto left-lateral strike-slip faults with a strike of 150° (Figure S2). (b) ΔCS resolved onto reverse-faulting earthquakes with a strike of 40°.

[e.g., *Hayes*, 2010; *Beavan et al.*, 2012]. The aftershocks are converted from point source moment tensor solutions to finite rectangular shear dislocation sources of equivalent moment with uniform slip. Empirical relations between magnitude and fault dimensions appropriate for South Island, New Zealand, earthquakes define the fault dimensions [*Yen and Ma*, 2011; *Stirling et al.*, 2013], and slip is computed from the seismic moment equation, assuming that the half-space has a shear modulus of 40 GPa (and a Poisson's ratio of 0.25). To compute Coulomb stress change (ΔCS) [*Reasenberg and Simpson*, 1992], shear and normal stresses are resolved at the location of a target structure, onto the geometry of the structure, with a coefficient of friction of 0.5. At each location, the stress change value is the cumulative sum of the stress change contributions from all of the preceding seismicity, beginning with the 3 September 2010 Darfield main shock. In particular, ΔCS is resolved onto both nodal planes of the February 2016 M_w 5.7 event. The earthquake is placed at its relocated epicenter (172.76°E, 43.50°S) at the centroid depth derived from the RMT analysis (9 km). This depth is very similar to the relocated hypocenter depth (8 km); therefore, the choice of centroid or hypocenter depth does not make a significant difference in the calculated ΔCS value for this event.

To explore what parts of the Canterbury Plains remain positively loaded, we also determine the cumulative ΔCS in the region from the 156 earthquakes from September 2010 up to (but not including) the February 2016 M_w 5.7 event and consider the additional ΔCS generated by the February 2016 event and its aftershocks. This regional ΔCS is computed at a depth of 10 km, the mean depth of our RMT centroids. We resolve the ΔCS onto three different fault orientations representing the dominant kinematic styles of the 2010–2013 Canterbury earthquakes: E-W right-lateral strike slip, NW-SE left-lateral strike slip, and NE-SW reverse faulting. The ΔCS distributions resolved onto right-lateral strike-slip and the conjugate left-lateral strike-slip faults are very similar, except for the details of the location and amplitude of stress change in close proximity to the earthquakes of the Canterbury sequence (Figure S2). These three fault orientations are also consistent with nearby structures imaged in reflection seismic surveys (Figure 3) [e.g., *Barnes et al.*, 2016]. With constraints on the kinematics and locations of faults in the Canterbury Plains from earthquakes and fault mapping, we can use ΔCS resolved onto these known target orientations to identify structures and areas that may have been loaded by the Canterbury sequence. This approach differs from studies that resolve the ΔCS on optimally oriented planes, which may not reflect existing structures [e.g., *Steacy et al.*, 2014]. We focus on the eastern end of the Canterbury sequence near Christchurch, because the ΔCS near the main shock rupture and in the broader Canterbury Plains region is dominated by the main shock and has been discussed in *Herman et al.* [2014].

Table 1. Regional Moment Tensor Solutions for the Nine Events From December 2013 to March 2016[a]

Label	Origin Time	Longitude	Latitude	Depth (km)	Strike	Dip	Rake	Magnitude
1	10/01/2014 02:33:54	172.386	−43.565	13	180	70	−10	3.9
2	29/03/2014 21:25:25	172.746	−43.595	12	185	70	40	3.7
3	12/09/2014 00:18:11	172.785	−43.152	11	20	50	75	3.9
4	12/12/2014 13:37:04	172.366	−43.639	7	0	85	−35	4.0
5	11/05/2015 18:54:25	172.068	−43.141	14	170	65	0	3.7
6	27/01/2016 23:24:42	172.517	−43.539	8	175	60	25	3.8
7	14/02/2016 00:13:43	172.762	−43.503	9	155	65	5	5.7
8	14/02/2016 05:27:49	172.818	−43.550	11	180	75	20	3.9
9	18/02/2016 06:17:42	172.757	−43.479	5	210	40	85	3.9
10	28/02/2016 14:32:40	172.635	−43.564	6	150	65	0	3.9
11	12/03/2016 10:01:31	172.799	−43.490	7	150	45	75	3.9

[a]The event labels correspond to those described in the text and in Figure 2b.

Finally, we explore the sensitivity of the ΔCS computation to variations in coefficient of friction (0.2–0.8), target fault depth (5–15 km), and main shock slip model (Figure S2) [*Hayes*, 2010; *Beavan et al.*, 2012].

3. Results

Relocation of the earthquake hypocenters provides us with an internally consistent catalog and does not significantly alter the general pattern of seismicity from the initial GNS Science locations (Figure 2a). The most noticeable change in the relocated catalog is that the earthquakes near Christchurch exhibit slightly greater levels of clustering, highlighting the primary structures hosting seismicity throughout the sequence. One area that might be expected to have some improved spatial coherence indicative of internal structure is the stepover feature near 172.4°E, which has been an area of intense and sustained activity throughout the Canterbury sequence [*Herman et al.*, 2014]. However, our relocated hypocenters do not appear to align in any systematic manner in the stepover region; this result suggests that whatever the internal structure is, the fault segments are short and spaced closer together than our phase arrival picks can resolve (<2 km). This interpretation is consistent with the relocations performed by *Syracuse et al.* [2013], in which they found hypocenters in the stepover clustered into three N-S oriented, vertically dipping planes ~2 km apart.

A primary motivation for this relocation exercise was to obtain a location for the 14 February 2016 M_w 5.7 event and its aftershocks consistent with and relative to previous events. The U.S. Geological Survey places its epicenter on the east (oceanside) of the NE-SW trend of reverse earthquakes offshore of Christchurch primarily associated with the 23 December 2011 event, while the GNS Science location for the event is immediately west (landside) of the reverse faulting structures. Our relocation is consistent with the GNS Science epicenter, placing the event closer to the intersection of the strike-slip faulting beneath southern Christchurch and the reverse faulting east of Christchurch (Figure 2a). The relocated epicenter of the February 2016 event is distinctly offset ~3 km west of the trend of reverse faulting aftershocks.

The 150 regional moment tensor (RMT) solutions for earthquakes in the Canterbury Plains from September 2010 to November 2013 (grey focal mechanisms in Figure 2b) [*Herman et al.*, 2014] were dominated by strike-slip faulting (W-E right lateral or NW-SE left lateral) and also included many oblique-reverse to reverse mechanisms, particularly at the eastern end of the sequence. Most of these events were consistent with a subhorizontal P axis oriented at ~115° [*Sibson et al.*, 2011; *Holt et al.*, 2013]. Here we have determined RMT solutions where possible, for any earthquake reported by GNS Science as M 4.0 or larger (http://www.geonet.org.nz) from January 2014 to April 2016. We found 11 events with waveforms suitable for RMT inversion, including the 14 February 2016 M_w 5.7 event and 10 more earthquakes with RMT magnitudes ranging from M_w 3.7 to 4.1 (Figure 2b and Table 1).

Six of these 11 earthquakes occurred prior to February 2016. These six events include three strike-slip earthquakes near the step over zone described in *Herman et al.* [2014], with magnitudes M_w 3.9 (January 2014; event 1 in Figure 2b and Table 1), 4.0 (December 2014; event 4), and 3.8 (January 2016; event 6). An M_w 3.7 strike-slip event (event 2) occurred in March 2014 under southern Christchurch, and an isolated M_w 3.9 reverse-faulting earthquake (event 3) occurred in September 2014 near the coast, north of Christchurch

(northeast of the region shown in Figure 2b). An M_w 3.7 strike-slip earthquake (event 5) occurred in May 2015 in the foothills of the Southern Alps, northwest of the main Canterbury sequence and associated with a cluster of seismicity that was active during the earlier sequence (north of the region shown in Figure 2b). These earthquakes have focal mechanisms that resemble the mechanisms of the earlier events in the Canterbury sequence: they are dominantly strike slip and also include oblique and reverse mechanisms.

The 14 February M_w 5.7 earthquake (event 7) occurred offshore east of Christchurch, near the region where the E-W trending right-lateral strike-slip structure under southern Christchurch (associated with the February 2011 event), the NW-SE left-lateral strike-slip structure extending onto Banks Peninsula to the south (associated with the June 2011 event), and the NE-SW trending reverse structure offshore east of Christchurch (associated with the December 2011 events) all intersect. The mechanism for this event is dominantly strike slip, with an orientation compatible with either of the conjugate strike-slip trends. Interpreting its fault plane is difficult because there is no clear surface evidence for the fault orientation, aftershocks do not clearly align with either nodal plane, and the event does not appear to fall on an extension of any of the previously ruptured structures. In particular, because the M_w 5.7 epicenter does not lie on a previously active trend of activity and has a strike-slip focal mechanism distinctly different from the nearby reverse-faulting earthquakes, we interpret that it occurred on a separate structure from the ones that have already hosted seismicity in the Canterbury sequence. Four of its aftershocks were large enough for RMT inversion (Figure 2b). The 14 February M_w 3.9 earthquake (event 8) 5 h following the main shock was a strike-slip event to the southeast of the main shock, and the 18 February M_w 4.0 earthquake (event 9) was a reverse-faulting event north of the main shock. Ten days later, on 28 February, an M_w 3.9 strike-slip faulting earthquake (event 10) occurred beneath western Christchurch. The most recent event for which we determined an RMT occurred on 12 March and was an M_w 3.9 reverse-faulting earthquake (event 11) offshore east of Christchurch. This earthquake had an unusual focal mechanism rotated nearly 90° from the orientation of other reverse-faulting earthquakes in this offshore segment.

The Coulomb stress change (ΔCS) resolved onto either nodal plane of the 14 February 2016 earthquake indicates that the event occurred in a region where previous events had reduced the stress levels. In general, the ΔCS is negative near locations where earthquakes have already occurred (Figure 3); however, it should be noted that the stress changes in the vicinity of previous ruptures vary from positive to negative over relatively short distances. Therefore, either nodal plane, small changes to the event location, dimensions or complexities of the source fault slip, or changes in frictional or elastic parameters may place the event into a ΔCS state of the opposite sign (Figure S2). This lack of resolvability of the ΔCS sign is common for events that occur very close to the source of stress change, especially for complex or multiple sources (e.g., foreshocks and aftershocks of the 2014 M_w 8.2 Iquique earthquake [*Hayes et al.*, 2014; *Herman et al.*, 2016]). Likewise, during the Canterbury sequence, much of the seismicity occurred near the rupture zone of one of the main events (the 2010 M_w 7.0 Darfield and 2011 M_w ~6.0 Christchurch earthquakes), and as a consequence, half of the Canterbury earthquakes occur in areas where the cumulative ΔCS from the preceding seismicity was negative [*Bebbington et al.*, 2016]. However, we find that all of the main Christchurch aftershocks (besides the February 2016 M_w 5.7 event) had positive cumulative ΔCS resolved onto their interpreted fault planes. These observations suggest that, although the capability to resolve ΔCS near the Canterbury earthquakes is not currently sufficient to understand the near-rupture aftershock activity, ΔCS appears to be an appropriate tool for anticipating earthquakes away from the rupture zones.

This provides motivation to examine stress changes in the regions farther from the already ruptured areas. The particular distribution of positive ΔCS depends on the target fault orientation, i.e., the style of faulting in the subsurface (Figure 3). Unlike the areas near the Canterbury earthquakes, these ΔCS regions tend to be robust with respect to changes in source or modeling parameters (Figure S2). One of the key areas of concern is under the city of Christchurch: whether potential fault structures here are strike slip or reverse (although few are mapped; Figure 3) [*Barnes et al.*, 2016], they appear to have been positively loaded. Similarly, the region east of the offshore structures has been positively loaded for structures with any of the kinematics observed in the Christchurch sequence. The main difference lies to the north: if the target structures north of the offshore events are strike slip, they have reduced ΔCS (Figure 3a), whereas reverse structures in this region have increased ΔCS (Figure 3b). Finally, adding the recent events does very little to change the general patterns of ΔCS, except in very close proximity to the event epicenter (within ~3 km).

Although ΔCS is not a predictive tool in the sense that it can tell us where and when the next significant earthquake will occur, it does suggest that Christchurch and the nearby vicinity should be considered as locations for possible continuing aftershock activity.

4. Discussion

A question about this sequence, that has been asked since the main shock ruptured on 3 September 2010, is when the sequence will finish [e.g., *Quigley et al.*, 2016]. Fitting the seismicity in the 150 days after the 2010 Darfield main shock with an Omori decay law [e.g., *Utsu et al.*, 1995] yields a decay exponent of ~0.9, and extrapolating this Omori fit, the seismicity rate returns to its pre-Darfield rate (~0.2 events per day) 20–30 years after the Darfield earthquake. However, the large 2011 Christchurch earthquake sequences, as well as the occurrence of several moderate to large earthquakes near Christchurch in 2012 and 2013, and now this M_w 5.7 event, complicate this simple decay scenario and suggest that the time frame for the completion of this intraplate earthquake sequence may be significantly longer [e.g., *Reyners et al.*, 2013]. This is consistent with aftershock duration-loading rate relationships: at the relatively slow deformation rate in the Canterbury Plains (16 nstrain/yr of maximum compression [*Wallace et al.*, 2007]), a longer aftershock period is expected (as compared to aftershocks in plate boundary settings [*Stein and Liu*, 2009]). One possible mechanism for such sustained activity is that there are numerous, relatively small structures in the Canterbury Plains that have been brought closer to failure by the preceding seismicity, and some of these loaded faults eventually fail in earthquakes.

The locations and mechanisms of the Canterbury earthquakes, including the recent February 2016 event, are consistent with this proposed mechanism: the earthquakes highlight a complex network of faults, suggesting that we should not think of the subsurface as containing only a few dominant structures but rather as densely populated with faults with multiple orientations, all of which can potentially slip in an earthquake. This interpretation of the subsurface structures from seismicity is also consistent with seismic reflection surveys in the Canterbury Plains that have imaged dense sets of faults both onshore [e.g., *Dorn et al.*, 2010] and offshore (Figure 3) [e.g., *Barnes et al.*, 2011, 2016]. The seismically imaged faults have strikes ranging from E-W to NE-SW, and there is likely another set of faults to accommodate left-lateral strike slip on NW-SE faults, as in the June 2011 event. Although some of these imaged segments appear to be relatively short (~5 km), empirical relations between magnitude and fault size suggest that a M_w 5.7 earthquake rupture area in South Island, New Zealand, has dimensions of 5 km by 5 km [*Yen and Ma*, 2011].

As the Coulomb stress change analysis demonstrates, the stress changes in the Canterbury Plains are significant and vary over relatively short spatial scales (Figure 3). Although the details of the Coulomb stress change cannot be precisely resolved because of the uncertainties inherent in the earthquake source characterization, event locations, and elastic properties, it seems likely that complex stress perturbations in a region containing many faults with diverse orientations would bring some of these faults closer to failure. In particular, although a structure might lie in a region where right-lateral strike-slip faulting is inhibited by stress changes from the Canterbury sequence, if it is a reverse fault, its kinematics might be favored by the stress changes. So although the sequence seems to be returning to relative quiescence, similar small to moderate earthquakes on nearby unmapped faults should be considered as a continuing hazard even when all of the primary structures, e.g., the Darfield fault, have apparently ruptured.

References

Barnes, P. M., C. Castellazzi, A. Gorman, and S. Wilcox (2011), National Institute of Water & Atmosphere (NIWA) client report WLG2011-28, Wellington, New Zealand: National Institute of Water and Atmospheric Research, submarine faulting beneath Pegasus Bay, offshore Christchurch. Short-term Canterbury Earthquake Recovery Project 2: Offshore Faults, p. 46.

Barnes, P. M., F. C. Ghisetti, and A. R. Gorman (2016), New insights into the tectonic inversion of North Canterbury and the regional structural context of the 2010-2011 Canterbury earthquake sequence, New Zealand, *Geochem. Geophys. Geosyst.*, 17, 324–345, doi:10.1002/2015GC006069.

Beavan, J., M. Motagh, E. J. Fielding, N. Donnelly, and D. Collett (2012), Fault slip models of the 2010–2011 Canterbury, New Zealand, earthquakes from geodetic data and observations of postseismic ground deformation, *N. Z. J. Geol. Geophys.*, 55, 207–221.

Bebbington, M., D. Harte, and C. Williams (2016), Cumulative Coulomb stress triggering as an explanation for the Canterbury (New Zealand) aftershock sequence: Initial conditions are everything?, *Pure Appl. Geophys.*, 173, 5–20.

Dorn, C., A. G. Green, R. Jongens, S. Carpentier, A. E. Kaiser, F. Campbell, H. Horstmeyer, J. Campbell, M. Finnemore, and J. Pettinga (2010), High-resolution seismic images of potentially seismogenic structures beneath the northwest Canterbury Plains, New Zealand, *J. Geophys. Res.*, 115, B11303, doi:10.1029/2010JB007459.

Fialko, Y. (2006), Interseismic strain accumulation and the earthquake potential on the southern San Andreas fault system, *Nature*, *441*, 968–971.

Fry, B., and W. C. Gerstenberger (2011), Large apparent stresses from the Canterbury earthquakes of 2010 and 2011, *Seismol. Res. Lett.*, *82*, 833–838.

Hayes, G. (2010), *M*7.0—South Island of New Zealand. U.S. Geological Survey (Web. 8 Apr. 2016. http://earthquake.usgs.gov/earthquakes/eqinthenews/2010/us2010atbj/finite_fault.php).

Hayes, G. P., M. W. Herman, W. D. Barnhart, K. P. Furlong, S. Riquelme, H. M. Benz, E. Bergman, S. Barrientos, P. S. Earle, and S. Samsonov (2014), Continuing megathrust earthquake potential in Chile after the 2014 Iquique earthquake, *Nature*, *512*, 295–298.

Herman, M. W., R. B. Herrmann, H. M. Benz, and K. P. Furlong (2014), Using regional moment tensors to constrain the kinematics and stress evolution of the 2010–2013 Canterbury earthquake sequence, South Island, New Zealand, *Tectonophysics*, *633*, 1–15.

Herman, M. W., K. P. Furlong, G. P. Hayes, and H. M. Benz (2016), Foreshock triggering of the 1 April 2014 M_w 8.2 Iquique, Chile, earthquake, *Earth Planet. Sci. Lett.*, *447*, 119–129.

Herrmann, R. B., H. Benz, and C. J. Ammon (2011), Monitoring the earthquake source process in North America, *Bull. Seismol. Soc. Am.*, *101*, 2609–2625.

Herrmann, R. B. (2013), Computer Programs in Seismology: An evolving tool for instruction and research, *Seismol. Res. Lett.*, *84*, 1081–1088.

Holt, R. A., M. K. Savage, J. Townend, E. M. Syracuse, and C. H. Thurber (2013), Crustal stress and fault strength in the Canterbury Plains, New Zealand, *Earth Planet. Sci. Lett.*, *383*, 173–181.

McCann, W. R., S. P. Nishenko, L. R. Sykes, and J. Krause (1979), Seismic gaps and plate tectonics: Seismic potential for major boundaries, *Pure Appl. Geophys.*, *117*, 1082–1147.

Okada, Y. (1992), Internal deformation due to shear and tensile faults in a half-space, *Bull. Seismol. Soc. Am.*, *82*, 1018–1040.

Quigley, M. C., M. W. Hughes, B. A. Bradley, S. van Ballegooy, C. Reid, J. Morgenroth, T. Horton, B. Duffy, and J. R. Pettinga (2016), The 2010–2011 Canterbury earthquake sequence: Environmental effects, seismic triggering thresholds and geologic legacy, *Tectonophysics*, *672–673*, 228–274.

Reasenberg, P. A., and R. W. Simpson (1992), Response of regional seismicity to the static stress change produced by the Loma Prieta earthquake, *Science*, *255*, 1687–1690.

Reyners, M., D. Eberhart-Phillips, and S. Martin (2013), Prolonged Canterbury earthquake sequence linked to widespread weakening of strong crust, *Nat. Geosci.*, *7*, 34–37.

Ristau, J., C. Holden, A. Kaiser, C. Williams, S. Bannister, and B. Fry (2013), The Pegasus Bay aftershock sequence of the M_w 7.1 Darfield (Canterbury), New Zealand earthquake, *Geophys. J. Int.*, *195*, 444–459.

Sibson, R., F. Ghisetti, and J. Ristau (2011), Stress control of an evolving strike-slip fault system during the 2010–2011 Canterbury, New Zealand, earthquake sequence, *Seismol. Res. Lett.*, *82*, 824–832.

Steacy, S., A. Jimenez, and C. Holden (2014), Stress triggering and the Canterbury earthquake sequence, *Geophys. J. Int.*, *196*, 473–480.

Stein, S., and M. Liu (2009), Long aftershock sequences within continents and implications for earthquake hazard assessment, *Nature*, *462*, 87–89.

Stirling, M., T. Goded, K. Berryman, and N. Litchfield (2013), Selection of earthquake scaling relationships for seismic-hazard analysis, *Bull. Seismol. Soc. Am.*, *103*, 2993–3011.

Syracuse, E. M., C. H. Thurber, C. J. Rawles, M. K. Savage, and S. Bannister (2013), High-resolution relocation of aftershocks of the M_w 7.1 Darfield, New Zealand, earthquake and implications for fault activity, *J. Geophys. Res. Solid Earth*, *118*, 4184–4195, doi:10.1002/jgrb.50301.

Utsu, T., Y. Ogata, and R. S. Matsuura (1995), The centenary of the Omori formula for a decay law of aftershock activity, *J. Phys. Earth*, *43*, 1–33.

Waldhauser, F., and W. L. Ellsworth (2000), A double-difference earthquake location algorithm: Method and application to the Northern Hayward Fault, California, *Bull. Seismol. Soc. Am.*, *90*, 1353–1368.

Wallace, L. M., J. Beavan, R. McCaffrey, K. Berryman, and P. Denys (2007), Balancing the plate motion budget in the South Island, New Zealand, using GPS, geological and seismological data, *Geophys. J. Int.*, *168*, 332–352.

Wessel, P., and W. Smith (1991), Free software helps map and display data, *Eos Trans. AGU*, *72*, 441, doi:10.1029/90EO00319.

Yen, Y.-T., and K.-F. Ma (2011), Source-scaling relationship for *M* 4.6-8.9 earthquakes, specifically for earthquakes in the collision zone of Taiwan, *Bull. Seismol. Soc. Am.*, *101*, 464–481.